Measurement of the $\overline{p}p \to K_sK_s$ Reaction from 0.6 to 1.9 GeV/c

C. Evangelista, A. Palano
University of Bari and INFN, Bari, Italy

D. Drijard, N. H. Hamann[†], R. T. Jones[*], B. Mouëllic, S. Ohlsson, J.-M. Perreau
CERN, Geneva, Switzerland

W. Eyrich, M. Moosburger, S. Pomp, F. Stinzing
University of Erlangen-Nürnberg, Erlangen, Germany

H. Fischer, J. Franz, E. Rössle, H. Schmitt, H. Wirth
University of Freiburg, Freiburg, Germany

A. Buzzo, K. Kirsebom, M. Lo Vetere, M. Macrì, M. Marinelli, S. Passaggio, M.G. Pia, A. Pozzo, E. Robutti, A. Santroni
University of Genova and INFN, Genova, Italy

P. T. Debevec, R. A. Eisenstein, P.G. Harris, D.W. Hertzog, S. A. Hughes, P. E. Reimer[**], J. Ritter
University of Illinois, Urbana, Illinois, USA

R. Geyer, K. Kilian, W. Oelert, K. Röhrich, M. Rook, O. Steinkamp
Institut für Kernphysik, Forschungszentrum Jülich, Jülich, Germany

H. Korsmo, B. Stugu
University of Oslo, Oslo, Norway

T. Johansson
Uppsala University, Uppsala, Sweden

(June 26, 1997)

The $\overline{p}p \to K_sK_s \to 4\pi^{\pm}$ cross section was measured at incident antiproton momenta between 0.6 and 1.9 GeV/c using the CERN Low Energy Antiproton Ring (LEAR). This investigation was part of a systematic study of in-flight antiproton-proton annihilations into two-neutral-meson final states in a search for hadronic resonances. A coarse scan of the $\overline{p}p \to K_sK_s$ cross section as a function of center-of-mass energy between 1.964 and 2.395 GeV/c^2 and a fine scan of the region surrounding the $\xi(2220)$ are presented. Upper limits on the product branching ratio $\mathrm{BR}(\xi \to \overline{\mathrm{p}}\mathrm{p}) \times \mathrm{BR}(\xi \to \mathrm{K_sK_s})$ are determined for a wide range of mass and width assumptions based on the non-observation of the $\xi(2220)$. A rise in the $\overline{p}p \to K_sK_s$ cross section is observed near 2.15 GeV/c^2, which is consistent with the $f_2(2150)$ resonance.

I. INTRODUCTION

Quantum Chromodynamics (QCD) has been very successful in describing the strong interaction at high energies. Within the framework of QCD, hadrons are composed of colored quarks (q), antiquarks ($\overline{q}$) and gluons (g) bound together into color neutral states. The experimentally observed families of bound states can be grouped and described in the framework of the naive quark model in which only three-quark (qqq) and quark-antiquark ($q\overline{q}$) constructions are used. The fact that gluons as well as quarks carry color charge in QCD means that they should appear along with quarks as valence particles in hadronic wavefunctions. QCD calculations on the lattice support the existence of states with valence glue and predict their masses with increasing reliability [1]. The experimental discovery of the glueball spectrum would greatly increase our understanding of the strong force at the hadronic scale [2].

While no gluonic state has been conclusively identified, several strong candidates exist. Good arguments have been made that one or both of the $f_0(1500)$ and the $f_J(1700)$ states might be a scalar gluonic state or at least mixed with such a state [3]. At higher mass, the flavor-neutral decay pattern and narrow width of the $f_J(2220)$, also known as

the $\xi(2220)$, have led to its identification as a possible tensor glueball [4]. Additionally, arguments have been made in support of the gluonic nature of the three broad tensor "g_T states" at masses of 2.010, 2.300, and 2.340 GeV [5].

The Jetset experiment was designed to search for such states by measuring the energy dependence of the total and differential cross sections of proton-antiproton annihilations into exclusive two-meson final states. The $\phi\phi$, K_sK_s and $\eta\eta$ final states were emphasized because of their suggested sensitivity to specific candidate resonances and their expected small non-resonant cross sections. Incident antiproton momenta from 0.6 to 1.9 GeV/c (1.964 to 2.395 GeV/c^2 in center-of-mass energy) were used. The choices of momenta provided both a broad scan of the entire energy region available at LEAR, as well as a more focused study in the vicinity of the $\xi(2220)$ state.

The $\xi(2220)$ was first reported by the Mark III collaboration in radiative J/ψ decays [6]. It appeared as a very narrow structure with a mass of 2.231 GeV/c^2 and a width of 0.020 GeV/c^2 in the reconstructed mass spectra of K^+K^- and K_sK_s from the decays $J/\psi \to \gamma K^+K^-$ and $J/\psi \to \gamma K_sK_s$. The quantum numbers allowed for this state are $J^{PC} = (\text{even})^{++}$. More recently, the BES experiment at Beijing reported [7] seeing the $\xi(2220)$ not only in $K\overline{K}$ decays but also in non-strange $J/\psi \to \gamma\pi\pi$ and $J/\psi \to \gamma\overline{p}p$ channels. In this context a measurement of the $\overline{p}p \to K_sK_s$ cross section in the region of the $\xi(2220)$ is of particular interest since both entrance and exit channels have been observed to couple to this state. A similar measurement has also been reported by the PS185 collaboration at LEAR [8]. In combination, these two experiments place strict limits on the production of the $\xi(2220)$ in this channel. Additional motivation for the experiment is drawn from the reported resonances in the $\phi\phi$ system at Brookhaven [5] in the reaction $\pi^-p \to n\phi\phi$ and from the fact that data on the meson spectrum from $\overline{p}p$ in-flight annihilations are comparatively scarce.

II. EXPERIMENT

Data were collected using a non-magnetic detector constructed around a hydrogen gas jet target installed in one of the straight sections of the CERN Low-Energy Antiproton Ring (LEAR). The detector was divided into a forward end-cap covering the region from 9° to 45° and a barrel sector covering 45° to 135°. Each region consisted of the following components: inner trigger scintillators, straw tracking chambers, silicon dE/dx pads, threshold Čerenkov counters, three layers of outer scintillators, and an electromagnetic calorimeter. A schematic view of the detector is shown in Fig. 1. More detailed descriptions of the detector may be found elsewhere [9] [10]. The hydrogen gas jet target had a density of up to 5×10^{12} atoms/cm^2 at the beam intersection. LEAR typically stored between 2.5 and 3.0×10^{10} antiprotons. With a revolution frequency of approximately 3.2 MHz at a momentum of 1.5 GeV/c, this leads to an instantaneous luminosity of approximately $4 \times 10^{29}\text{cm}^{-2}\text{s}^{-1}$. The fractional momentum uncertainty was less than 0.1% or approximately 0.5 MeV in center-of-mass energy.

The prominent feature of $\overline{p}p \to K_sK_s \to 4\pi^{\pm}$ events is the relatively long lived K_s which has a mean lifetime, τ, of 0.08926 ns, or $c\tau = 2.676$ cm [11]. This allowed the K_s mesons to travel a macroscopic distance before decaying. This feature was exploited to detect and identify K_sK_s events. The tracks made by the charged pions from the K_s decay formed an unmistakable V^0 pattern in the detector. The online identification of K_s event candidates looked for these delayed decays by requiring signals in the outer scintillators and the Čerenkov counters for each of the charged pions while using the inner scintillators which surrounded the interaction region as a veto shield. This ensured that at least the forward-going pair of pions was produced outside of the target region.

Data with the K_s trigger were collected in July and October of 1991. The July data set consisted of eight evenly spaced momenta between 1.2 and 1.9 GeV/c, referred to as the "coarse scan." The October "fine scan" data included seven momenta from 1.39 to 1.48 GeV/c in 0.015 GeV/c steps, covering the $\xi(2220)$ mass region. In addition, K_s data at 0.61 and 0.85 GeV/c were obtained during special calibration runs at the start of the October period.

III. DATA ANALYSIS

The reconstruction of events depended on the identification of a delayed K_s decay vertex. Charged particle tracks were reconstructed based on information from the straw tracking chambers. To form two independent vertices, four tracks were required. An event sample with four or five tracks was examined for vertex combinations. Vertices were divided into two categories: those made of two forward tracks, and those made of two barrel tracks[1]. In each event,

[1]Vertices formed from one forward and one barrel track were not used. The additional acceptance (less than 10%) owing to this topology was overwhelmed by the increase in background. No clean extraction of such events was possible.

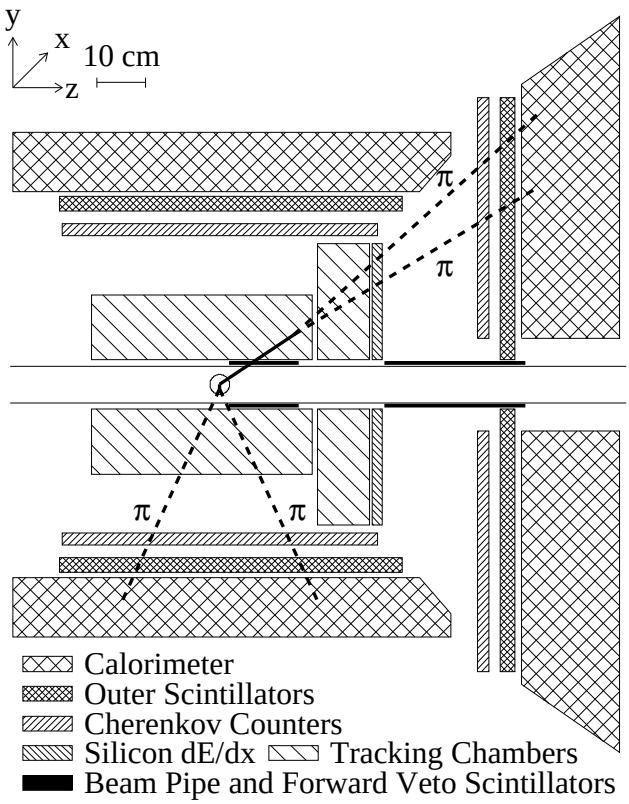

FIG. 1. Schematic view of the Jetset detector with a K_sK_s event superimposed.

forward and barrel vertex candidates were made by matching all pairs of forward or barrel tracks. Candidate vertices were removed if the distance of closest approach of the two tracks was greater than 3.06 cm or 5.89 cm for forward and barrel vertices, respectively, or if the plane defined by the two tracks did not contain the target.

The barrel tracker straw wires provided modest (1.3 cm) position resolution in the z direction through charge division and good ($150-500$ μm) resolution in the orthogonal coordinates (xy) from the drift-time information. The latter fact was exploited to make a test of momentum conservation in the xy plane of the barrel K_s decay vertex by requiring that it is possible to draw a line from the interaction region to the vertex, which extends through the opening of the V^0. Barrel vertices failing this test were discarded. Once identified, each candidate vertex was geometrically fit. The tracks from the fit vertex were followed outward. If either track passed through an inner scintillator, which should have vetoed the event, the vertex was removed. This eliminated vertices made by random coincidences of tracks which at some point along their trajectories passed the distance of closest approach and other cuts mentioned earlier. Events with less than two independent vertices and events containing photons, identified by the calorimeter, were removed from the event sample.

The momentum of each tracked pion was not directly measured, but was determined through solution of momentum and energy conservation in the event. This solution assumed that the reconstructed tracks were produced by pions and was based on the measured directions of the particles. For each event, up to two solutions could be consistent with the kinematics. Owing to the finite detector resolution, a "violation" of energy conservation for a candidate solution was permitted up to $0.2 \times E_{beam}$. Monte Carlo studies verified the placement of this cut. For events with no solutions, either the hypothesis that the tracks were produced by pions was wrong, or there were other, unobserved final state particles in the event. In either case, these events were removed from the event sample.

A least squares fit to the kinematics of $\overline{p}p \to K_sK_s \to 4\pi^{\pm}$ was performed for each event having an allowable momentum solution. The kinematic fit provided improved precision for the momenta of the pion tracks, and yielded a measure of the probability that the event matched the $\overline{p}p \to K_sK_s \to 4\pi^{\pm}$ hypothesis. The χ^2 distribution is shown in Fig. 2. For both data and Monte Carlo events, the χ^2 distribution was found to be broader than that expected for an *ideal* least squares fit with six degrees of freedom. This was not surprising owing to effects such as multiple-scattering and pion interactions. When compared in detail, the Monte Carlo and data χ^2 distributions have a nearly identical shape, however with the scale stretched by a factor of 5.5 for the real events. This factor

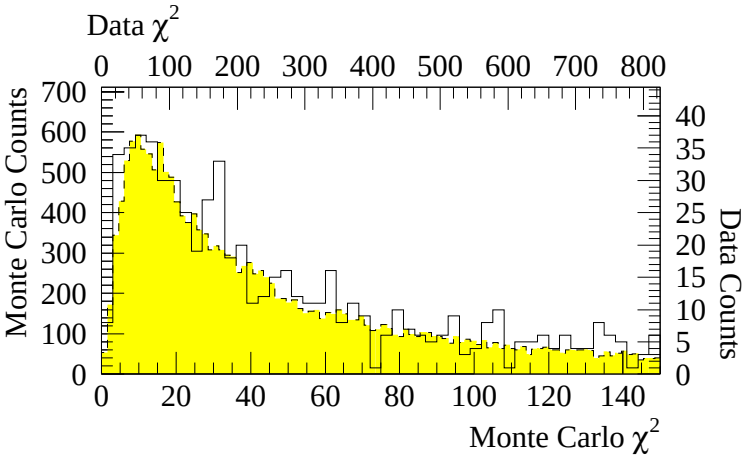

FIG. 2. χ^2 distributions for data (unshaded, solid line) and Monte Carlo events (shaded, dashed line). The lower and left scales are for the Monte Carlo events and the upper and right scales are for data.

comes from consideration of the additional non-Gaussian uncertainties which are present in the detector but which were not included in the simulation. For example, the precision of the positioning of the forward and barrel trackers with respect to one another was worse than the resolution of these devices. Further, the true straw-tracker resolution function had to be described by two Gaussians, one narrow and one broad. In the simulation, only an average was used. Both effects were studied and were found to contribute to the χ^2 scale difference. The maximum allowed χ^2 in the final data sample was set to 825 which was large enough so that the scale difference did not affect any of our conclusions beyond the systematic errors we report.

These steps led to the following reduction in the number of events. The fraction of two-vertex candidate events in the raw trigger was 0.045% and 0.079% for the fine- and coarse-scan data sets, respectively. This difference is understood and is described later. Of the 6195 fine-scan and 11,442 coarse-scan events which remained, approximately 16% were left once the photon cut was applied. Events with candidate kinematical solutions lowered the sample to approximately 9%. Finally, after the kinematic fitting and χ^2 cuts were applied 159 fine-scan and 346 coarse-scan events remained. We estimate that approximately 90% of these events were $\overline{p}p \to K_sK_s$ events as discussed below.

A plot of the invariant mass for the forward vertex versus that of the barrel[2] is shown in Fig. 3 for events which, when processed by the event fitting routine, were found to have an acceptable χ^2. The plot is dominated by events in the K_sK_s mass region. Evidence for a small background contamination can be seen in the regions on the high-mass sides of the peak. The background events are primarily from the $\overline{p}p \to K_sK^* \to K_sK_s\pi^0$ and $\overline{p}p \to K_sK^* \to K_sK^{\pm}\pi^{\mp}$ reactions and their non-resonant partners, which can easily mimic the channel of interest. These reactions have cross sections from 10 to 100 times larger than the $\overline{p}p \to K_sK_s$ cross section [12]. The final states involving neutral π^0 are identified and rejected when one or more photons were observed in the calorimeter. Monte Carlo studies of simulated background events processed according to the K_sK_s hypothesis confirmed that a small number do enter the final sample and that the invariant mass reconstruction for these events is always on the high side of the K_s mass as seen in the plot.

The number of background events was estimated by comparing the decay length distribution with the ideal one for true K_s decays. The measured decay lengths, converted to a lifetime distribution, should show an exponential decay. Any deviation from this due to events with charged particles emerging directly from the origin shows up as an excess at very small lifetimes, while the tail of the distribution is unaffected. The background was estimated by fitting the tail of the lifetime distribution and extrapolating into the region where the prompt V^0 decays create an excess. The exact shape of the distribution for the delayed decays was determined by Monte Carlo taking into account the full acceptance of the detector.

This method of estimating the number of background events in the sample depends on having a statistically significant number of events in the tail of the lifetime distribution. For this purpose, the data were divided into

[2]The kinematics of $\overline{p}p \to K_sK_s$ forbids events with both vertices in the barrel region or both vertices in the forward region, except in rare instances at the 1.9 GeV/c incident momentum setting.

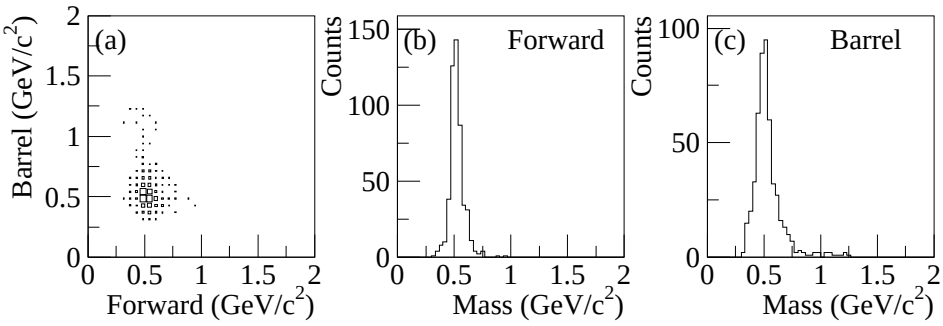

FIG. 3. Goldhaber plot of invariant mass combinations formed from forward and barrel vertices. This plot represents all of the data where a solution has been found with two independent vertices.

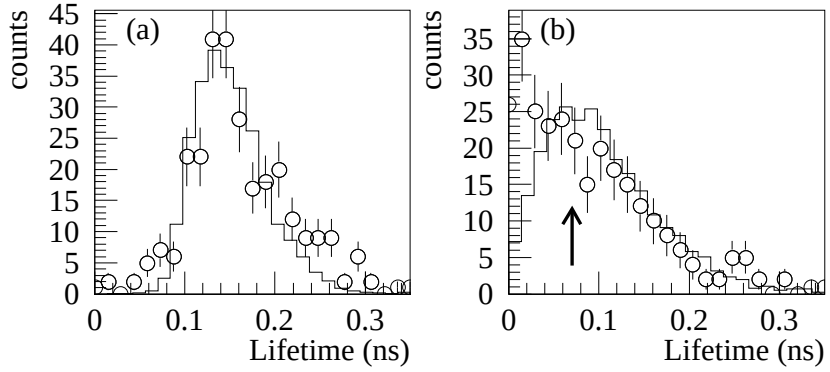

FIG. 4. Lifetime distributions for the fine-scan data (points) and Monte Carlo (histogram) for forward (a) and barrel (b) vertices. The arrow indicates where the "tail" began for purposes of the fit.

three groups: the 1.6 to 1.9 GeV/c coarse-scan data, the 1.2 to 1.5 GeV/c coarse-scan data and the fine scan (1.39 to 1.50 GeV/c). Even with this division, the statistics in the tail region were limited, and a "binned likelihood" procedure based on Poisson statistics was used for the fit [13]. The only parameter varied in this fit was an overall scale factor for the Monte Carlo distributions. Based on this procedure, the event samples contained $(89.1 \pm 9.3)\%$, $(91.8 \pm 7.2)\%$ and $(91.5 \pm 8.9)\%$ true $\overline{p}p \to K_sK_s$ events for the three samples, respectively. Fig. 4 shows the lifetime distributions for the fine-scan data along with a corresponding Monte Carlo distribution which has been scaled by the fitting procedure described.

The Monte Carlo events were generated using the GEANT package from CERN [14]. The geometry and composition of all detectors and relevant support structures were included in the simulation. Monte Carlo events for the reaction $\overline{p}p \to K_sK_s$ were generated isotropically in $\cos(\theta_{cm})$ and then weighted according to the second order Legendre polynomial fit reported by the PS185 collaboration for their data obtained near 1.43 GeV/c incident antiproton momentum [8]. Since the true K_sK_s differential cross section rises slightly at forward angles, this procedure resulted in an increase in the inferred total cross section by an average of 4% compared to what would have been obtained assuming a flat differential cross section. The Monte Carlo events passed through the same analysis steps outlined above to determine the overall detector acceptance. Events from relevant background reactions such as $\overline{p}p \to K_sK^*$ were also generated with a uniform angular distribution and were studied for feed-down into the K_sK_s sample.

The integrated luminosity at each momentum setting was determined by continuously measuring the $\overline{p}p$ elastic differential cross section at 90° in the center-of-mass frame. The absolute cross section for elastic scattering is well established throughout the energy region of interest [15]. A special trigger, based on pairs of pixels in the forward outer scintillator array, was used to select these events and a separate analysis was performed on this data sample. A comparison of the acceptance-corrected elastic yield to the published cross section provided a measure of the absolute integrated luminosity. An additional 15% uncertainty, not included in the errors on the individual points, exists on the scale of our final cross sections and is common for all of the energy points. This systematic error includes 5% uncertainty on the $\overline{p}p$ elastic cross sections. The relative energy-point to energy-point integrated luminosity is more precise and was derived not only from the elastic event sample, but also from a combination of trigger scintillator

Beam Momentum (GeV/c)	Center of Mass Energy (GeV/c^2)	Integrated Luminosity (nb^{-1})	Monte Carlo Accept. (%)	Num. of Events	Cross Section (μb)
Coarse Scan					
1.900	2.395	3.59	0.31	1	0.17 ± 0.17
1.800	2.360	20.75	0.31	41	1.21 ± 0.23
1.700	2.324	11.17	0.32	25	1.33 ± 0.30
1.600	2.289	19.48	0.33	65	1.90 ± 0.31
1.500	2.254	4.13	0.35	9	1.22 ± 0.42
1.400	2.218	13.71	0.33	69	2.95 ± 0.43
1.300	2.183	16.10	0.33	77	2.84 ± 0.40
1.200	2.149	4.75	0.30	59	8.16 ± 1.26
Fine Scan					
1.480	2.247	8.62	0.085	17	1.71 ± 0.45
1.465	2.241	6.06	0.092	20	2.67 ± 0.66
1.450	2.236	11.29	0.085	29	2.17 ± 0.46
1.435	2.231	11.57	0.085	36	2.63 ± 0.52
1.420	2.225	11.92	0.092	38	2.56 ± 0.49
1.405	2.220	5.30	0.085	15	2.44 ± 0.68
1.390	2.215	1.49	0.085	4	2.28 ± 1.17
Additional Points					
0.850	2.033	1.76	0.037	7	6.04 ± 2.76
0.609	1.964	1.03	0.018	2	6.07 ± 5.06

TABLE I. The $\overline{p}p \to K_sK_s$ cross sections. Also listed are the integrated luminosity, the acceptance, the number of events detected at each energy and the fraction of those events which are $\overline{p}p \to K_sK_s \to 4\pi^{\pm}$ events.

scalers which were found to be very reliable and stable for the lifetime of the Jetset experiment. The relative luminosity error was found to be approximately 2%.

IV. RESULTS AND DISCUSSION

The total cross section as a function of the center-of-mass energy was derived by dividing the background-subtracted number of observed events by the integrated luminosity and by the acceptance. The results are listed in Table I and are shown in Fig. 5. The measured cross section is interpreted as the sum of contributions from a smoothly-varying, non-resonant production plus any resonances. The exact form of the non-resonant component of the cross section, σ_{nr}, is not important as it changes only slightly over the region of interest and several functional forms can be used. However, we find it convenient to employ the parametrization of Vandermeulen [16], which recognizes that $\overline{N}N$ annihilations proceed dominantly through two-meson intermediate states. It has the form

$$\sigma_{nr} = Ap^* \times e^{-Bp^*}, \tag{1}$$

where A and B are parameters, and p^* is the momentum of the K_s mesons in the center-of-mass, $p^* = (1/2) \times \sqrt{s - 4m_{K_s}}$. The solid line in Fig. 5 follows this form and fits the data well.

Between the coarse-scan and fine-scan runs, the radiator in the Čerenkov counters was changed from FC72 [17] to water with a corresponding decrease in the threshold β from $0.79 \times c$ to $0.75 \times c$. This detector was designed to be used as a veto for fast pions ($\beta > 0.9$) in a trigger for the reaction $\overline{p}p \to 4K^{\pm}$ which was a primary channel of our experiment. To keep the fraction of false fast-pion vetos low, the discriminator thresholds on these detectors were raised so that $25 - 50\%$ of the fast charged pions passed through undetected. This change in threshold happened when between the coarse- and fine-scan runs. The consequence to the K_sK_s data set was an inefficiency in the trigger for the fine scan. Since the thresholds were comfortably below pion threshold during the coarse scan, we choose to normalize the fine-scan data to the coarse-scan data to establish the final cross section values. The ratio

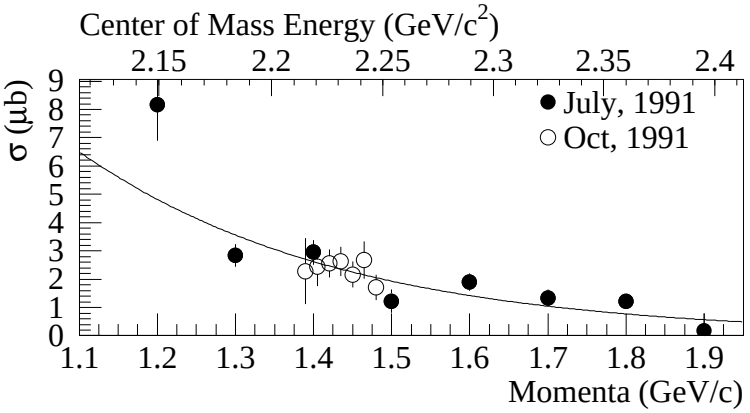

FIG. 5. Total cross section for the reaction $\overline{p}p \to K_sK_s$. The solid curve is a fit following the form $Ap^* \times e^{-Bp^*}$, excluding the 1.2 GeV/c point. The fine-scan data have been adjusted to match the scale of the coarse-scan by means of a multiplicative factor.

$A_{coarse}/A_{fine} = 0.61 \pm 0.07$ was used. In the search for narrow resonances in the fine-scan data, this normalization factor does not influence the relative cross section data, only the scale.

To calculate the differential cross section with sufficient statistics, the data were summed into the three groups mentioned above. These distributions are shown in Fig. 6. The angular acceptance of the detector limited the range of the differential cross section to $0.3 < cos(\theta_{cm}) < 0.9$. In the region of the acceptance, all of the distributions show little structure. A Legendre polynomial fit was not done due to the limited data near $cos(\theta_{cm}) = 1$, which is needed in order to include the higher-order terms.

The resonant portion of the cross section, if present, may be described by a Breit-Wigner line shape. If there is no interference between the resonance and the background, then these contributions can be summed. The Breit-Wigner parametrization is given by

$$\sigma_{BW} = (w_i w_f) \times \frac{(2J+1)}{(2S_1+1)(2S_2+1)} \times \frac{4\pi(\hbar c)^2}{s - 4m_p^2} \times \frac{\Gamma^2}{(\sqrt{s} - m_{res})^2 + \Gamma^2/4}. \quad (2)$$

Here $(w_i w_f)$ is the double branching ratio and $w_i w_f = \mathrm{BR(X \to \overline{p}p)} \times \mathrm{BR(X \to K_sK_s)}$. The S_i terms are the spins of the initial proton and antiproton (1/2), and J is the total angular momentum of the resonance, reducing the angular momentum term, $(2J+1)/\left((2S_1+1)(2S_2+1)\right)$ to either 5/4 or 9/4 for $J = 2$ or $J = 4$. With these parametrizations of the non-resonant and resonant cross sections, the total cross section may be expressed as a function of five parameters: A and B from Eq. 1 and $(w_i w_f)$, Γ and m_{res} from Eq. 2. To completely describe the data, a sixth parameter was added to renormalize the fine scan to the coarse-scan data.

For fixed mass and width assumptions, the likelihood ratio test was used to place limits on the strength of a possible resonance [18]. In this test, an initial likelihood fit was made in which the strength of the resonance was allowed to vary freely. The fit was then repeated with a fixed resonance strength, $(w_i w_f)^*$. The likelihood ratio is defined as $\lambda = \frac{L^*}{L}$, where the likelihood from the initial fit is L and the likelihood from the fit with fixed resonance strength is L^*. The significance of the resonance strength, $(w_i w_f)^*$, can be deduced by noting that the statistic $-2\ln\lambda$ follows a χ^2 distribution with one degree of freedom. The resonance strength was systematically increased and new fits were made until the resonance strength corresponding to a significance 0.05 was found. This strength represents an upper limit on the double branching ratio with confidence of 95% for the particular mass and width which were chosen.

In the region of the ξ, this procedure was performed for widths in the range from 5 to 40 MeV/c^2 and masses from 2.219 to 2.246 GeV/c^2. The composite results are compiled in Fig. 7a in the form of a contour map representing upper limits on the double branching ratio as a function of resonance width and mass. A tensor ($J = 2$) resonance was assumed. For a $J = 4$ resonance, the upper limit must be multiplied by the factor 5/9 to account for the spin term in Eq. 2. The least restrictive limit on a possible resonance as determined by this data set alone occurs at a mass of 2.231 GeV and a width of 0.012 GeV. Here, the upper limit on the double branching ratio is 19.5×10^{-5}. A fit of the cross section which forces a resonance at this point produces a double branching ratio of approximately 5×10^{-5} with a significance of just less than one standard deviation.

A similar analysis was made for the cross section measurements presented here combined with those reported by the PS185 collaboration [8] which cover the same general energy region, however at slightly different specific momentum

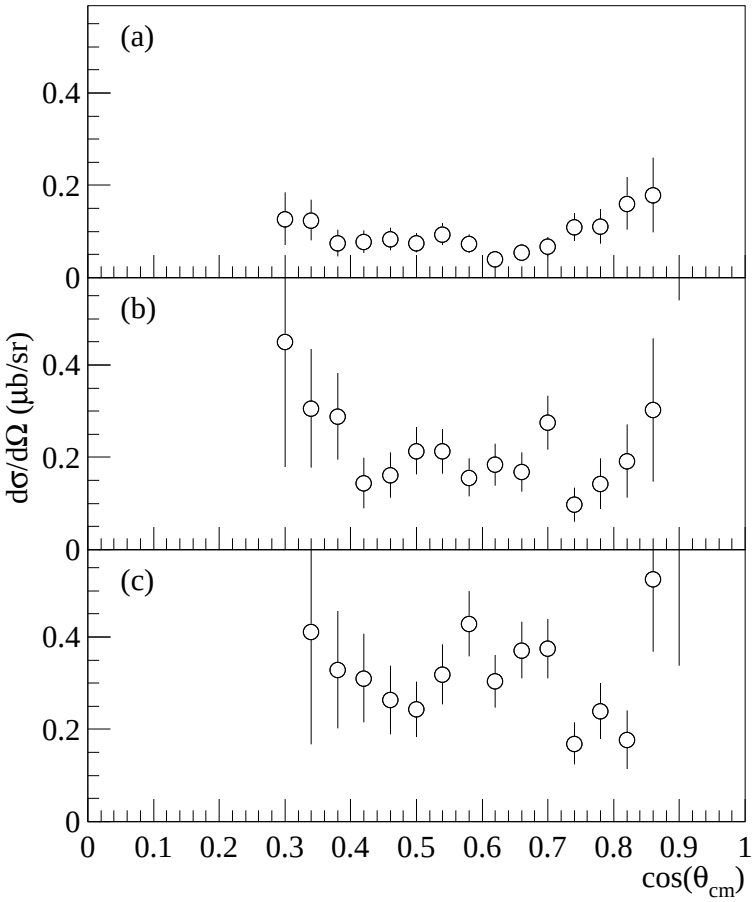

FIG. 6. Differential cross section results for three energy groupings of the reaction $\overline{p}p \to K_sK_s$. The 1.2, 1.3, 1.4 and 1.5 GeV/c data are shown in (a), the fine scan 1.39-1.48 GeV/c data are shown in (b) and the 1.6, 1.7, 1.8 and 1.9 GeV/c data are shown in (c).

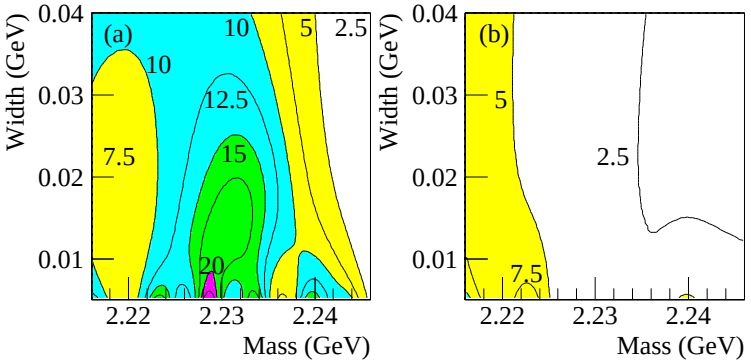

FIG. 7. Contours of the upper limit on the double branching ratio BR($\xi \to \overline{\mathrm{p}}\mathrm{p}$) × BR($\xi \to \mathrm{K_sK_s}$) as a function of resonance mass and width for a $J = 2$ resonance. The contours represent steps of 2.5×10^{-5} and the shading changes in steps of 5×10^{-5}. In (a) only the data from this work are considered. In (b) our data are combined with the data from PS185 [8] and the same procedure is repeated.

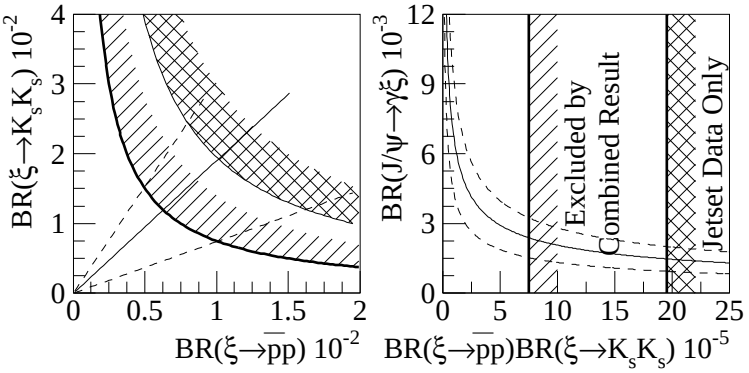

FIG. 8. Regions of allowed branching ratios. The solid lines represent the observed strengths of coupling of the ξ to K_sK_s (MARK III and BES) and $\overline{p}p$ (BES only). The dashed lines are 1σ limits. A portion of each plot is excluded by use of the Jetset data alone (cross hatched). Significantly tighter limits are set by the combined Jetset/PS185 data (single hatched).

values. Merging the two data sets required an additional parameter to account for the 15% uncertainty in the global normalizations reported as systematic errors in the overall cross section scale by each experiment. The contours for the combined data are shown in Fig. 7b. Some insensitive regions exist where neither experiment accumulated data, however generally the limits[3] on the double branching ratio are relatively constant at less than 7.5×10^{-5} for a resonance whose width is greater than 5 MeV/c^2.

These results may be combined with those from Mark III and BES to establish allowed values for the single branching ratios BR(J/$\psi \to \gamma\xi$), BR($\xi \to$ K$_s$K$_s$) and BR($\xi \to \overline{\rm p}$p). Plotted in Fig. 8a are the single branching ratios BR($\xi \to$ K$_s$K$_s$) versus BR($\xi \to \overline{\rm p}$p). The K_sK_s are averaged from MARK III and BES, while the $\overline{p}p$ result is from BES alone[4]. The results presented here form a hyperbola which sets an upper bound on the product, implying that single branching ratios up to the 1 to 2% limit are allowed. Very large couplings are excluded. In Fig. 8b, the same information is used to show the region permitted for the coupling $J/\psi \to \gamma\xi$. In the allowed region, the branching ratio is greater than 0.2% which indicates a very strong coupling. An upper limit on BR(J/$\psi \to \gamma\xi$) may also be inferred based on the total of all radiative decays which is approximately 8%.

An examination of the broad scan reveals that the $\overline{p}p \to K_sK_s$ cross section at 1.2 GeV/c (2.148 GeV/c^2) appears significantly larger than is expected with the simple non-resonant parametrization. During the period of the fine scan, data were collected at two additional momenta below 1.2 GeV/c. These data, 0.61 and 0.85 GeV/c, were used for detector calibration. The $\overline{p}p \to K_sK_s$ trigger was in operation, but the luminosity trigger was not. The integrated luminosity for these points was deduced by comparing the counting rates in simple coincidences formed by various triggering counters with those obtained at other momenta where the integrated luminosity was known. An extrapolation was used for the anticipated momentum-dependence of the rates. The final values for these low-momentum points are given in Tab. I where the errors not only reflect the small number of events, but also the additional uncertainties in the integrated luminosity and acceptance.

A complete view of the $\overline{p}p \to K_sK_s$ total cross section is seen in Fig. 9 where all the world's data are represented. A resonance in the region of the 1.2 GeV/c point has been reported in several other channels including $\overline{p}p \to \pi^0\pi^0$ [28], $\overline{p}p \to \overline{p}p$ [29], $\overline{p}p \to \overline{n}n$ [30], and the $\overline{p}p$ total cross section [31]. All find evidence for a structure near 2.150 GeV with a statistically consistent width in the range from 0.050 to 0.250 GeV/c^2. The fit by the BES collaboration of the $\overline{p}p$ spectrum in $J/\psi \to \gamma\overline{p}p$ also included such a structure at 2.144 GeV/c^2 [7]. A 2^{++} resonance, known as the $f_2(2150)$, is associated with this collection of observations by the Particle Data Group [11]. When the data below 1.8 GeV/c^2 in the $\overline{p}p \to K_sK_s$ summary are fit with a freely floating Breit-Wigner permitted to sum incoherently with the background, one finds that the data is consistent with this resonance, having a double branching ratio of

[3]The 3σ limits quoted in Ref. [8] are more restrictive than those produced by the likelihood method when applied to either the PS185 data alone, or to the combined PS185/Jetset data. A constrained background function was used in the PS185 fitting procedure which may contribute in part to the difference. We judge the likelihood method and results to be more general in nature and properly representative of the true limits implied by these searches for the ξ.

[4]MARK III set a limit of BR(J/$\psi \to \gamma\xi$) $\times$ BR($\xi \to \overline{\rm p}$p) $< 2 \times 10^{-5}$ at a confidence limit of 90%. BES measured 1.5×10^{-5} for the same quantity based on a peak with a 3.8 standard deviation significance.

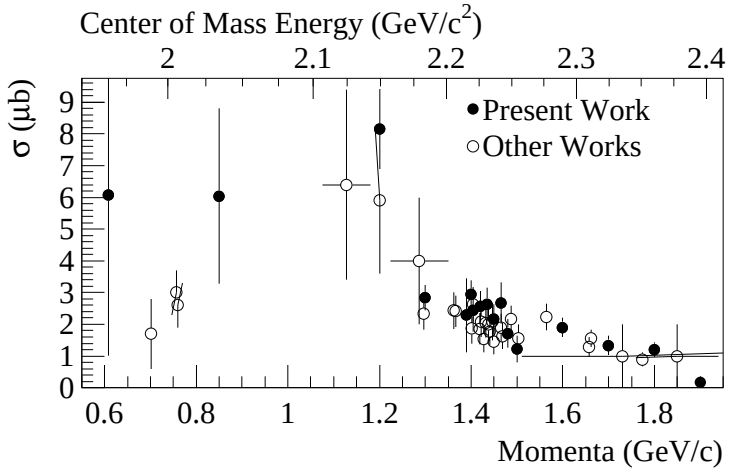

FIG. 9. The world's data for the reaction $\overline{p}p \to K_sK_s$. Other data are taken from Refs. [8,12,19-27].

$(w_i w_f) = (27^{+9}_{-7}) \times 10^{-5}$ at $2.139^{+0.008}_{-0.009}$ GeV/c^2 having a width of $0.056^{+0.031}_{-0.016}$ GeV/c^2. The χ^2 per degree of freedom for this fit was 28.9/40 compared with 60.7/43 when fit with no resonance.

V. CONCLUSIONS

We have reported new results on a search for the $\xi(2220)$ in the formation channel $\overline{p}p \to K_sK_s$. No evidence for the $\xi(2220)$ was found. Combining these results with those from earlier work at LEAR by the PS185 experiment [8] sets new limits on the double branching ratio product BR($\xi \to \overline{\rm p}$p) $\times$ BR($\xi \to {\rm K_sK_s}$) for a wide range of mass and width assumptions of the ξ. For mass and width combinations appropriate to the radiative J/ψ findings, the double branching ratios are all less than 7.5×10^{-5} at a confidence level of 95%. The implications of this limit are that the coupling of the $\xi(2220)$ to the final states $K\overline{K}$ and $\overline{p}p$ is very small, at the level of 1% or less. Given these results in combination with other measurements of the $\xi(2220)$, the question arises, if the channels in which the $\xi(2220)$ has been observed are not its primary decay modes, to which channels does it strongly couple? In a study of the $\pi^0\pi^0$, $\eta\eta$ and $\phi\phi$ final states, our experiment establishes similar limits [32]. If the $\xi(2220)$ does indeed couple to $\overline{p}p$ at the level reported by BES, then greater than 90% of its decays have yet to be discovered.

VI. ACKNOWLEDGMENTS

We thank the teams of the CERN Antiproton Complex, in particular the LEAR staff. This work has been supported in part by CERN, the German Bundesministerium für Bildung, Wissenschaft, Forschung und Technologie, the Italian Istituto Nazionale di Fisica Nucleare, the Swedish Natural Science Research Council, the Norwegian Research Council, and the United States National Science Foundation, under contract NSF PHY 94-20787. This work was based in part on the dissertation of P. E. Reimer, submitted to the University of Illinois in partial fulfillment of the requirements for the Ph.D. degree.

---

† Deceased.
* Present Address: University of Connecticut, Storrs, CT.
** Present Address: Los Alamos National Laboratory, Los Alamos, NM.

[1] G. S. Bali *et al.*, Phys. Lett. B **309** (1993) 378; and J. Sexton, A. Vacarino and D. Weingarten, Phys. Rev. Lett. **75** (1995) 4563.

[2] F. E. Close, Rep. Prog. Phys. **51** (1988) 833; and T. H. Burnett and S. R. Sharpe, Annu. Rev. Nucl. Part. Sci. **40** (1990) 327.
[3] C. Amsler and F. Close, Phys. Lett. **B353** (1995) 3858; C. Amsler and F. Close, Phys. Rev. **D53** (1996) 295; and J. Sexton, A. Vacarino and D. Weingarten, Phys. Rev. Lett. **75** (1995) 4563.
[4] T. Huang, S. Jin, D. Zhang, K. Chao, Phys. Lett. **B380** (1996) 189.
[5] A. Etkin *et al.*, Phys. Lett. **B165** (1985) 217, and A. Etkin *et al.*, Phys. Lett. **B201** (1988) 568.
[6] R. M. Baltrusaitis *et al.*, Phys. Rev. Lett. **56** (1986) 107.
[7] J. Z. Bai *et al.*, Phys. Rev. Lett. **76** (1996) 3502.
[8] P. D. Barnes *et al.*, Phys. Lett. **B309** (1993) 469.
[9] C. Evangelista *et al.*, Phys. Lett **B345** (1995) 325; and C. Evangelista *et al.*, *The $\overline{p}p \to \phi\phi$ reaction near threshold,* CERN SPSLC 92-42, SPSLC M501 (10 August 1992).
[10] P. E. Reimer, Ph.D. Thesis, University of Illinois, 1996.
[11] Particle Data Group, Phys. Rev. **D54**, (1996) 1.
[12] V. Flaminio *et al.*, Compilation of Cross-Sections III: p and $\overline{p}$ Induced Reactions, CERN-HERA 84-01 (17 April 1984).
[13] R. Barlow and C. Beeston, Comp. Phys. Comm. **77** (1993) 219; and F. James, Minuit: Function Minimization and Error Analysis, CERN (1994).
[14] Application Software Group, Computing and Networks Division, GEANT: Detector Description and Simulation Tool, (CERN, Geneva, Switzerland, 1993).
[15] E. Eisenhandler *et al.*, Nucl. Phys. **B113** (1976) 1-33; T. Bacon *et al.*, Nucl. Phys. **B32** (1971) 66-74; and D. L. Parker *et al.*, Nucl. Phys. **B32** (1971) 29-44.
[16] J. Vandermeulen, Z. Phys. **C37** (1988) 563.
[17] FC72 is the trade name of a compound marked by 3M composed of C_6F_{14}, sometimes known as "liquid freon."
[18] A. G. Frodesen, O. Skjeggestad, and H. Tøfte, **Probability and Statistics in Particle Physics**, Bergen: Universitetsforlaget, 1979.
[19] S. N. Ganguli *et al.*, Nucl. Phys. **B183** (1981) 295-329.
[20] A. M. Cooper *et al.*, Nucl. Phys. **B136** (1978) 365.
[21] J. Duboc *et al.*. Nucl. Phys. **B46** (1972) 429.
[22] J. Barlow *et al.*, Nuovo Cimento **A50** (1967) 701.
[23] T. Handler *et al.*, Nucl. Phys. **B110** (1976) 173-88.
[24] B. Y. Oh *et al.*, Nucl. Phys. **B51** (1973) 57.
[25] R. Todenhagen, Ph. D. Thesis, Albert-Ludwigs-University, Freiburg, Germany, 1995.
[26] J. W. Chapman *et al.*, Nucl. Phys. **B42** (1972) 1.
[27] T. Fields *et al.*, Phys. Lett. **B40** (1972) 503.
[28] R. S. Dulude *et al.*, Phys. Lett. **B79** (1978) 335.
[29] M. Coupland *et al.*, Phys. Lett. **B71** (1977) 460.
[30] D. Cutts *et al.*, Phys. Rev. **D17** (1978) 16.
[31] J. Alspector *et al.*, Phys. Rev. Lett. **30** (1973) 511.
[32] A. Buzzo *et al.*, in preparation.